journal

J. Am. Ceram. Soc., 96 [1] 201–208 (2013)
DOI: 10.1111/jace.12019

Investigation of the Structure and Electrical Properties of $(K_xNa_{0.96-x}Li_{0.04})(Nb_{0.96-y}Ta_ySb_{0.04})O_3$ Piezoelectric Ceramics Modified with Manganese

Henry E. Mgbemere,[‡] Manuel Hinterstein,[§] and Gerold A. Schneider[‡,†]

[‡]Institute of Advanced Ceramics, Hamburg University of Technology, Hamburg, Germany

[§]Institut für Werkstoffwissenschaft, Technische Universität Dresden, Dresden, Germany

The effect of high doping levels of manganese (Mn) on the structure and electrical properties of $(K_xNa_{1-x})NbO_3$ (KNN) ceramics containing Li, Ta, and Sb has been investigated. The samples were measured using synchrotron X-ray diffraction whereas Rietveld refinement with Fullprof was used to determine the structural information as a function of temperature. Temperature-dependent dielectric measurement was used to compare the phase transition temperatures. The results show that Mn decreases the temperature range of phase coexistence between the orthorhombic and tetragonal phase from ~180°C to ~120°C. The Curie temperature remained unchanged with Mn addition while the dielectric constant and dielectric loss increased with Mn addition. High amounts of Mn led to a reduction in both piezoelectric and ferroelectric properties. The remnant polarization, remnant strain, and piezoelectric coefficient values decreased from 24 μC/cm², 0.000824, 338 ± 37 pm/V to 13 μC/cm², 0,00014 and 208 ± 27 pm/V, respectively for the undoped and 5 mol% Mn-doped sample.

I. Introduction

Substitution of KNN ceramics with both aliovalent and isovalent elements has been reported to increase its piezoelectric coefficients (d_{33}) while also making the sintering process easier.[1–4] An orthorhombic-tetragonal phase coexistence has been reported when 5–7 mol% of Li is used to dope KNN ceramics. A second phase related to $K_3Li_2NbO_5O_{15}$ is observed with more than 7 mol%.[2] A series of phase changes has been observed for Li-doped KNN ceramics (0–10 mol%) from low temperatures to temperatures above their T_c using a combination of Raman spectroscopy, X-ray diffraction, and dielectric constant studies.[5] A piezoelectric coefficient (d_{33}) value of 405 pC/N has been reported for (001) oriented single crystal of KNN ceramics doped with Li using the Bridgman method.[6] The reported dielectric constant value was, however, very low. Addition of Ta to KNN ceramics has been reported to result in the softening of the sample leading to improvements in the d_{33}, coupling factors, dielectrics properties while decreasing the coercive field (E_c), and quality mechanical factors.[7] It has been used to produce an electro-holographic crystal for optical application.[8] A comprehensive study of KNN ceramics doped with Li and Ta has been reported by Saito and Takao.[9] Phase boundaries between orthorhombic and tetragonal phases were observed with changing amounts of Li and Ta and the reported highest piezoelectric coefficient value ($d_{33} \sim 230$ pm/V) was obtained with $((K_{0.5}Na_{0.5})_{0.97}Li_{0.03})(Nb_{0.8}Ta_{0.2})O_3$ composition. Abnormal core-shell structure which has been interpreted using the classical grain growth theory just like in $BaTiO_3$ has been reported both for Li- and Ta-doped KNN [10] and for KNN with a combination of 7 mol% $LiTaO_3$ and 5 mol% $BiScO_3$.[11] KNN ceramics doped with Li and Sb has been studied and a phase boundary between an orthorhombic and a tetragonal phase was observed between 4 and 6 mol%.[12] KNN ceramics modified with a combination of Li, Ta, and Sb abbreviated here as KNNLST was reported by Saito *et al.*[13] to have high piezoelectric coefficients, which are comparable to values from lead-containing ceramics. Consequently, the research interest in KNN ceramics containing these substituents has been high.

Manganese (Mn) is an interesting element with multivalent ions and has been used to dope piezoelectric ceramics to improve their piezoelectric properties, to reduce the conductivity, and to improve the sinterability. It has been reported to cause "hard" effects in $Pb(Zr_xTi_{1-x})O_3$ and $BaTiO_3$-based ceramics mainly due to the size of the ionic radius which favors its incorporation into the B-site of the perovksite lattice.[14,15] It also acts as a domain pinning element and causes strong aging in $Pb(Mg_{0.33}Nb_{0.66})O_3$ ceramics.[16] Mn has also been used to dope $(Bi_{0.5}Na_{0.5})TiO_3$ (BNT)-based ceramics and the results vary depending on the authors. Li *et al.*[17] reported that the electrical properties deteriorated whereas Fan *et al.*[18] reported that both hard and soft ferroelectric effects were obtained. Aksel *et al.*[19] using electron paramagnetic resonance (EPR), reported that the valence state of Mn in BNT ceramics depends strongly on the thermal treatment stating that it is oxidized and reduced after calcination and sintering processes, respectively.

Manganese has been used to modify KNN-based ceramics and it is believed to enter both the A and B-sites of the lattice.[20–22] Improved dielectric constant, decreased peak intensity ratio (I_{220}/I_{002}), and a mixture of orthorhombic and tetragonal phases have been reported for $0.95Na_{0.5}K_{0.5}NbO_3$–$0.05LiTaO_3$ ceramics doped with ≤ 1 mol% MnO.[23] KNN single crystals doped with Mn showed that the leakage current was suppressed and EPR measurements indicate that this is due to oxidation of Mn.[24,25] When added in very small amounts to KNN ceramics, the resistivity and electromechanical quality factor are improved while the dielectric loss values are reduced. Higher piezoelectric coefficient and dielectric permittivity values have been reported.[26] The objective of this research was to investigate both the structure and electrical properties of KNNLST ceramics doped with relatively high amounts of Mn to determine its solubility limit and effect on the ceramics.

II. Experimental Procedure

(1) Sample Preparation

The compositions which were intended to be produced using the mixed-oxide synthesis method are $(K_{0.48}Na_{0.48}Li_{0.04})(Nb_{0.86}Ta_{0.1}Sb_{0.04})O_3$, $(K_{0.47}Na_{0.47}Li_{0.04})(Nb_{0.85}Ta_{0.1}Sb_{0.04})O_3$–$Mn_{0.015}$, $(K_{0.47}Na_{0.47}Li_{0.04})(Nb_{0.84}Ta_{0.1}Sb_{0.04})O_3$–$Mn_{0.02}$,$(K_{0.46}$

W. K. Wong-Ng—contributing editor

Manuscript No. 31270. Received April 3, 2012; approved September 6, 2012.
†Author to whom correspondence should be addressed. e-mail: g.schneider@tu-harburg.de

$Na_{0.46}Li_{0.04})(Nb_{0.82}Ta_{0.1}Sb_{0.04})O_3$–$Mn_{0.05}$, $(K_{0.43}Na_{0.43}Li_{0.04})(Nb_{0.77}Ta_{0.09}Sb_{0.036})O_3$–$Mn_{0.1}$. K_2CO_3, Na_2CO_3, Li_2CO_3 (99%), Sb_2O_3, Nb_2O_5, Ta_2O_5 (99.9%) (Chempur Feinchemikalien und Forschungs GmbH, Karlsruhe, Germany), and MnO_2 (Merck Chemicals, Darmstadt, Germany) are the raw powders used. The powders were milled for 2 h and calcined for 4 h at 850°C. The milling and calcination process were repeated to ensure a homogeneous powder mixture and to reduce the particle size. After cold isostatic pressing at 300 MPa for 2 min, the pelletized samples were sintered at temperatures between 1050°C and 1090°C for 1 h. Samples for synchrotron X-ray were ground and annealed at 900°C for 4 h. Polarization hysteresis measurements were carried out at room temperature using the standard Sawyer-Tower circuit while both unipolar and bipolar strain hysteresis measurements were made using an inductive transducer device. A complete dipolar hysteresis measurement was performed in 200 sec.

The amounts of each element present in the samples were analyzed after sintering with Optical emission spectroscopy-Inductive coupled plasma (OES-ICP; PE-Optima 7000 DV, Perkin Elmer, Waltham, MA). A mean value was obtained from four separate measurements and the OES-ICP values as well as the element amount in moles are presented in Table I.

The amounts of Na, Ta, and O in most cases either remained unchanged or slightly higher than the calculated amounts before the synthesis whereas Li and K had lower amounts. The actual compositions were adjusted to reflect the changes in the amounts of elements present after the chemical analysis. ZrO_2 balls were used during the milling process and the chemical analysis showed that small amounts of ZrO_2 were present. The actual compositions are: $(K_{0.47}Na_{0.51}Li_{0.03})(Nb_{0.85}Ta_{0.1}Sb_{0.04})O_3$ abbreviated as KNNLST-0 mol% Mn, $(K_{0.444}Na_{0.505}Li_{0.034})(Nb_{0.822}Ta_{0.11}Sb_{0.04})O_{3.028}$–$Mn_{0.014}$ as KNNLST-1.5 mol% Mn, $(K_{0.453}Na_{0.498}Li_{0.034})(Nb_{0.823}Ta_{0.11}Sb_{0.04})O_{3.02}$–$Mn_{0.024}$ as KNNLST-2 mol% Mn, $(K_{0.448}Na_{0.536}Li_{0.035})(Nb_{0.762}Ta_{0.107}Sb_{0.041})O_{3.021}$–$Mn_{0.048}$ as KNNLST-5 mol% Mn, and $(K_{0.417}Na_{0.501}Li_{0.034})(Nb_{0.719}Ta_{0.101}Sb_{0.039})O_{3.079}$–$Mn_{0.107}$ as KNNLST-10 mol% Mn.

(2) Synchrotron X-Ray Data Collection and Refinement

The synchrotron X-ray diffraction data were collected at the synchrotron facility (beamline B2, HASYLAB/DESY) in Hamburg from 27°C to 400°C in steps of 20°C. High temperature measurements were performed using a capillary furnace from Stoe & Cie type 0.65.3. The data were recorded using a position sensitive image plate detector (OBI, *ortsfest auslesbarer Bildplattendetektor*)[27] at a wavelength of 0.6881 Å. More details about the experimental setup at the beamline can be found in the literature.[27,28] All the collected data were refined by the Rietveld method using the software package FULLPROF.[29]

The background under the peaks was refined using a linear interpolation between points from the regions in which no reflections contributed to the intensity. The model used was based on a T–C–H pseudo-Voigt profile function, which is convoluted with asymmetry due to axial divergence as formulated by Laar and Yelon[30] and using the method of Finger *et al.*[31,32] The atomic positions and the isotropic atomic displacement parameters B_{iso} were refined. The anisotropic peak broadening model in the general strain formulation from Stephens was used to refine the strain in the sample.[33]

All the patterns were refined using a two-phase model containing an orthorhombic (*Amm*2) and a tetragonal (*P*4*mm*) phase. Two of the fundamental translation vectors in *Amm2* are along the cubic {110} directions, instead of all three to be along {100} as in *P4mm* or *Pmm2*. The argument for using *Amm2* has been explained in a previous article.[34] In *Amm2,* the different values of b_o and c_o lead to a rhombic distortion of the $(001)_c$ plane resulting in an expansion along $[110]_c$. The

Table I. OES-ICP Analysis Data as well as Calculated Molar Amounts of the Elements in our Composition

Element	Li	Na	K	Nb	Ta	Sb	Mn	O	Zr*
$(K_{0.48}Na_{0.48}Li_{0.04})(Nb_{0.86}Ta_{0.1}Sb_{0.04})O_3$									
OES-ICP values (g/kg)	1.290 (4)	64.70 (12)	103.3 (10)	437.0 (7)	99.8 (5)	25.3 (7)		265	0.4
Element amount (mol)	0.0336	0.5086	0.4761	0.8501	0.0997	0.0376		2.9935	0.0008
$(K_{0.47}Na_{0.47}Li_{0.04})(Nb_{0.85}Ta_{0.1}Sb_{0.04})O_{2.97}$-0.015 MnO_2									
OES-ICP values (g/kg)	1.31 (1)	64.3 (17)	96.1 (4)	423 (6)	111 (6)	27.7 (7)	4.4 (1)	268	0.8
Element amount (mol)	0.03407	0.50495	0.44375	0.82229	0.1104	0.04099	0.01446	3.02756	0.00151
$(K_{0.47}Na_{0.47}Li_{0.04})(Nb_{0.84}Ta_{0.1}Sb_{0.04})O_{2.96}$-0.02 MnO_2									
OES-ICP values (g/kg)	1.33 (0)	64.1 (5)	99.1 (5)	428 (7)	111 (1)	28.1 (0)	7.27 (12)	270	0.6
Element amount (mol)	0.03425	0.49844	0.45311	0.82267	0.1098	0.04126	0.02364	3.01568	0.00115
$(K_{0.46}Na_{0.46}Li_{0.04})(Nb_{0.82}Ta_{0.1}Sb_{0.04})O_{2.9}$-0.05 MnO_2									
OES-ICP values (g/kg)	1.37 (1)	70.2 (2)	99.7 (2)	403 (6)	110 (2)	28.4 (1)	15.2 (1)	275	0.6
Element amount (mol)	0.03457	0.53638	0.44802	0.7625	0.1065	0.04093	0.04848	3.0214	0.0012
$(K_{0.43}Na_{0.43}Li_{0.036})(Nb_{0.77}Ta_{0.09}Sb_{0.036})O_{2.8}-0.1MnO_2$									
OES-ICP values (g/kg)	1.4 (1)	68.1 (2)	96.5 (2)	395 (12)	108 (1)	28.4 (1)	34.9 (1)	291	0.8
Element amount (mol)	0.034	0.50084	0.4174	0.71902	0.1008	0.03947	0.10749	3.07962	0.0014

refinement was done for each composition from 27°C to temperatures above their respective Curie temperatures (T_c). Single and two-phase refinement models were used depending on phase coexistence in the sample and the temperature of measurement. Orthorhombic, tetragonal, and cubic phases with space groups *Amm*2, *P*4*mm,* and $Pm\bar{3}m$, respectively, were used for the refinement. For phase coexistences, a two-phase model consisting of a combination of the respective models was used. Mn was incorporated to the B-site of the lattice for refinement purposes because its incorporation to the A-site did not give good results. The refinement results for the lowest temperature phase of each model used in the refinements are shown in Tables II, III, IV, and V for KNNLST-0 mol% Mn, KNNLST-1.5 mol% Mn, KNNLST-5 mol% Mn, and KNNLST-10 mol% Mn, respectively

(3) Temperature-Dependent Measurement of Dielectric Properties

To compare the phase transition temperatures observed with X-rays, temperature-dependent dielectric measurements were carried out. The surface of the pellets, which acted as electrodes for the measurement were coated with silver paint. The measurements were made using an LCR meter (HP 4284A; Agilent Technologies, Inc., Palo Alto, CA) connected to a heating chamber.

III. Results

The profiles for the measured and calculated diffraction patterns taken at 27°C and their difference for the samples are shown in Fig. 1. The inset in the figures shows the enlarged section of the patterns with 2θ values (19°–26°) highlighting the differences in the patterns with increasing amount of Mn. The lattice parameters as a function of temperature for the samples are shown in Fig. 2. The subscripts 'c', 'o', and 't' denote the cubic, orthorhombic, and tetragonal unit cells, respectively. The orthorhombic cell parameters b_o and c_o were divided by $(2)^{1/2}$ for better representation in the graphs. The KNNLST-0 mol% Mn plot [Fig. 2(a)] shows that the orthorhombic and tetragonal phase coexists between 27°C and 180°C. Only the tetragonal phase is present between 200°C and 340°C, whereas the cubic phase is observed from

Table II. Experimental Details and Refinement Results for KNNLST-0 mol% Mn Ceramics at 27°C, 200°C, and 360°C

Phase type	Two-phase		Single	Single
Crystal system	Orthorhombic	Tetragonal	Tetragonal	Cubic
Space group	*Amm2*	*P4mm*	*P4mm*	*Pm-3m*
Temperature (°C)	27	27	200	360
a (Å)	3.95129 (5)	3.96287 (8)	3.96152 (3)	3.97596 (16)
b (Å)	5.6391 (3)			
c (Å)	5.6437 (3)	4.00053 (18)	3.99759 (4)	
V (g/cm^3)	125.750 (9)	62.826 (3)	62.7369 (9)	62.8532 (4)
Z	2	1	1	1
Atomic positions				
O1 (z)	0.291 (6)	0.56 (2)	0.561 (4)	0
O2 (z)	0.574 (4)	0.00 (6)	0.003 (10)	
A-site atom (z)	0	0	0	0
B-site atom (z)	0.524 (3)	0.50 (2)	0.515 (4)	0.5
Refinement				
R_B (%)	3.89	5.69	8.02	7.31
R_f (%)	3.16	3.86	6.71	6.73
GOF	4.6		26.3	32
χ^2	21.5		5.1	5.6
No. of parameters	39		47	24

Table III. Experimental Details and Refinement Results for KNNLST-1.5 mol% Mn Ceramics at 27°C, 120°C, 320°C, and 340°C

Phase type	Two-phase		Single	Two-phase		Single
Crystal system	Orthorhombic	Tetragonal	Tetragonal	Tetragonal	Cubic	Cubic
Space group	*Amm2*	*P4mm*	*P4mm*	*P4mm*	*Pm-3m*	*Pm-3m*
Temperature (°C)	27	27	120	320	320	340
a (Å)	3.94963 (6)	3.95393 (5)	3.95716 (2)	3.97221 (4)	3.97146 (12)	3.973122 (17)
b (Å)	5.62324 (11)	–	–	–	–	–
c (Å)	5.64367 (9)	4.00092 (10)	4.00201 (4)	3.97725 (12)	–	–
V (g/cm^3)	125.345 (4)	62.5487 (20)	62.6680 (8)	62.755 (2)	62.640 (3)	62.7185 (5)
Z	2	1	1	1	1	1
Atomic positions						
O1 (z)	0.258 (8)	0.521 (3)	0.550 (5)	0.528 (17)	0.00000	0.00000
O2 (z)	0.54096 (5)	−0.013 (13)	0.028 (7)	0.00 (4)		
A-site atom (z)	0.00000	0.00000	0.00000	0.00000	0.00000	0.00000
B-site atom (z)	0.496 (3)	0.476 (3)	0.502 (5)	0.499 (16)	0.50000	0.50000
Refinement						
R_B (%)	6.59	–	8.51	8.57	6.5	8.12
R_f (%)	5.04	–	6.67	10.2	4.78	10
GOF	4.3	–	4.8	–	4.9	5
χ^2	18.7	–	23	–	24.5	24.6
No. of parameters	36	36	31	31	31	21

Table IV. Experimental Details and Refinement Results for KNNLST-5 mol% Mn Ceramics at 27°C, 100°C, 340°C, and 360°C

Phase type	Two-phase		Single	Two-phase		Single
Crystal system	Orthorhombic	Tetragonal	Tetragonal	Tetragonal	Cubic	Cubic
Space group	*Amm2*	*P4mm*	*P4mm*	*P4mm*	*Pm-3m*	*Pm-3m*
Temperature (°C)	27	27	100	340	340	360
a (Å)	3.94890 (6)	3.95780 (10)	3.95792 (4)	3.97472 (10)	3.97255 (12)	3.97567 (2)
b (Å)	5.62238 (12)	–	–	–	–	–
c (Å)	5.64632 (10)	3.9945 (3)	4.00162 (5)	3.9828 (2)	–	–
V (g/cm^3)	125.361 (4)	62.570 (5)	62.6858 (11)	62.921 (4)	62.692 (3)	62.8394 (7)
Atomic positions						
O1 (z)	0.252 (5)	0.5161 (20)	0.547 (6)	0.50 (4)	0.00000	0.00000
O2 (z)	0.54083 (10)	−0.079 (13)	0.026 (9)	−0.05 (2)		
A-site atom (z)	0.00000	0.00000	0.00000	0.00000	0.00000	0.00000
B-site atom (z)	0.4908 (20)	0.464 (6)	0.504 (5)	0.51 (2)	0.50000	0.50000
Z	2	1	1	1	1	1
Refinement						
R_B (%)	4.73	3.83	4.83	9.97	9.99	5.68
R_f (%)	4.08	3.77	4.3	7.62	9.15	5.42
GOF	3.6	–	3.8	4.6	–	4.3
χ^2	12.8	–	14.5	21	–	18.3
No. of parameters	36	–	31	31	–	21

Table V. Experimental Details and Refinement Results for KNNLST-10 mol% Mn Ceramics at 27°C, 120°C, and 340°C

Phase type	Two-phase		Single	Single
Crystal system	Orthorhombic	Tetragonal	Tetragonal	Cubic
Space group	*Amm2*	*P4mm*	*P4mm*	*Pm-3m*
Temperature (°C)	27	27	120	340
a (Å)	3.94795 (5)	3.96002 (12)	3.95814 (3)	3.97441 (2)
b (Å)	5.62364 (12)	–	–	–
c (Å)	5.64535 (8)	3.9751 (5)	4.00008 (5)	–
V (g/cm^{-3})	125.337 (4)	62.336 (8)	62.6689 (10)	62.7798 (6)
Z	2	1	1	1
Atomic positions				
O1 (z)	0.264 (5)	0.524 (2)	0.536 (8)	0.00000
O2 (z)	0.54086 (12)	0.275 (13)	0.028 (10)	0.00000
A-site atom (z)	0.00000	0.00000	0.00000	0.00000
B-site atom (z)	0.498 (2)	0.488 (7)	0.503 (6)	0.50000
Refinement				
R_B (%)	5.12	4.73	5.83	5.92
R_f (%)	4.04	3.43	4.59	5.55
GOF	3.8	–	3.9	4.3
χ^2	14.1	–	15.1	18.5
No. of parameters	36	–	31	21

360°C. The addition of 1.5 mol% Mn [Fig. 2(b)], decreases the temperature ranges of the phase coexistence from 180°C to 100°C. The tetragonal phase is present from 120°C to 300°C whereas the cubic phase is present from 320°C. For the KNNLST-5 mol% Mn sample [Fig. 2(c)], the two-phase region exists from 27°C to 120°C. The tetragonal phase is observed from 140°C to 320°C and at 340°C, the refinement was better when the tetragonal and cubic phase models are combined whereas the cubic phase is observed from 360°C. With the KNNLST-10 mol% Mn sample [Fig. 2(d)], there is a scatter in the tetragonal cell parameters a_t and c_t from 27°C to 60°C possibly due to large compressive stresses. A two-phase coexistence is observed from 27°C to 120°C and between 140°C and 320°C, the tetragonal phase is present. From 340°C, the cubic phase is present.

The weight fraction (%) of the constituent phases coexisting in the samples are calculated from the scale factors, which involve the product of the mass and volume of the unit cell contents of each phase. For KNNLST samples with 0 and 1.5 mol%, the fraction of the orthorhombic phase is slightly higher than that for the tetragonal phase up to 60°C and as the temperature increases, the fraction of the tetragonal phase becomes higher. With KNNLST-5 mol % Mn sample, the fraction of the orthorhombic phase content increases to ~ 80% at 27°C. As the temperature increases, the fraction of the tetragonal phase gradually increases and at 80°C, approximately equal fractions of both phases are observed. The content of the tetragonal phase approaches 90% at 120°C. For the KNNLST-10 mol% Mn sample, the fraction of the orthorhombic phase is ~90% at 27°C. As the temperature increases, the fraction of the tetragonal phase also increases and at 100°C, both phases are approximately equal. This indicates that although Mn decreases the temperature range of phase coexistence, it increases the weight fraction of the orthorhombic phase at temperatures below 100°C.

The plot of the dielectric constant values of KNNLST ceramics modified with Mn is shown in Fig. 3(a). The insets highlight the behavior of the samples at temperatures below 250°C. Higher dielectric constant and dielectric loss values [Fig. 3(b)] are observed for the samples modified with Mn at temperatures below 75°C compared to the undoped sample.

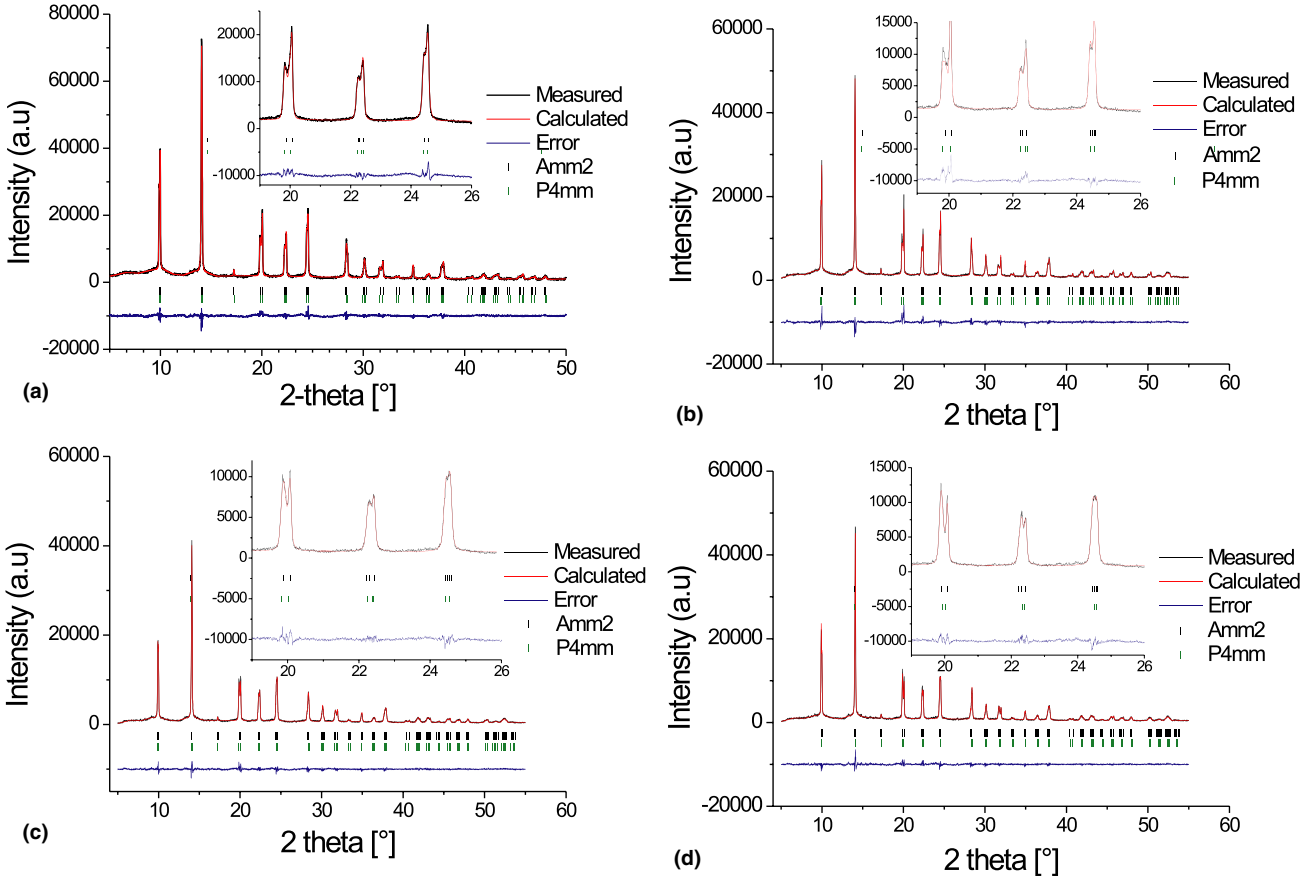

Fig. 1. Measured and calculated X-ray diffraction profiles and their difference plot at 27°C for KNNLST ceramics with (a) 0 mol% Mn, (b) 1.5 mol% Mn, (c) 5 mol% Mn, and (d) 10 mol% Mn, respectively.

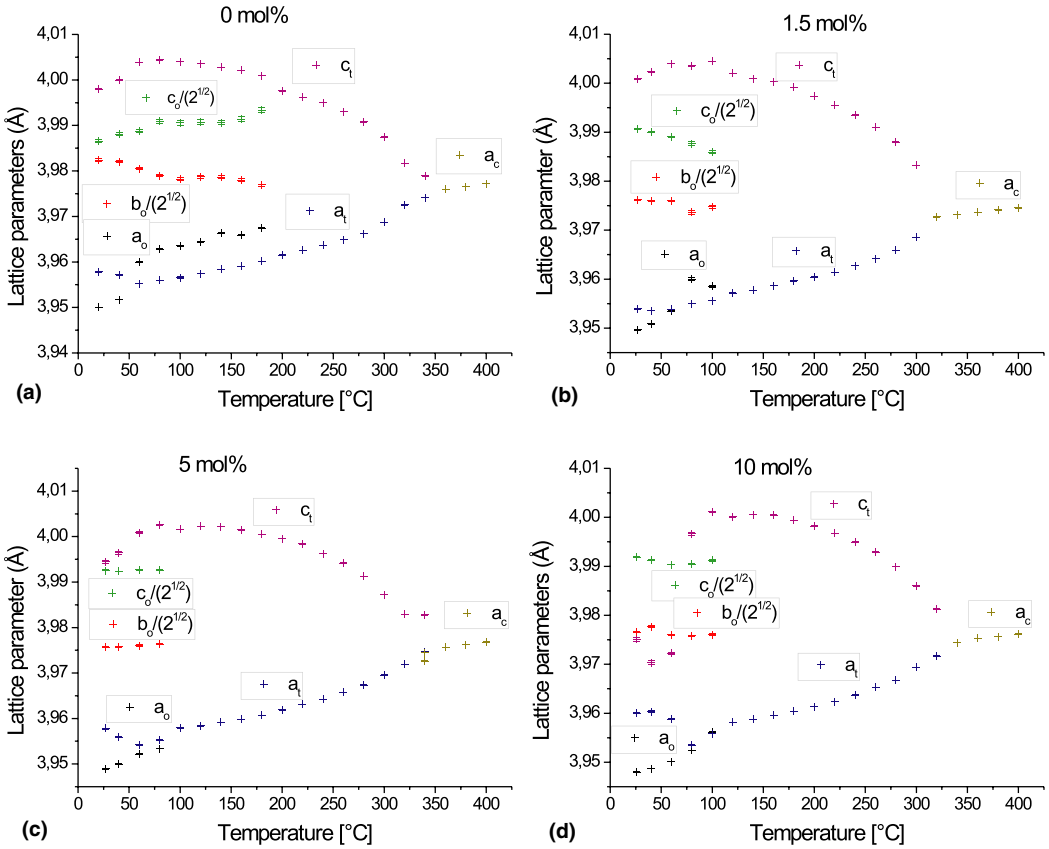

Fig. 2. Lattice parameters (Å) of the samples as a function of temperature. a_o, b_o, and c_o represent the parameters for the orthorhombic phase, a_t and c_t represent the parameters for the tetragonal phase whereas a_c represents the cubic phase, respectively. The graphs are for (a) KNNLST-0 mol% Mn, (b) KNNLST-1.5 mol% Mn, (c) KNNLST-5 mol% Mn, and (d) KNNLST-10 mol% Mn.

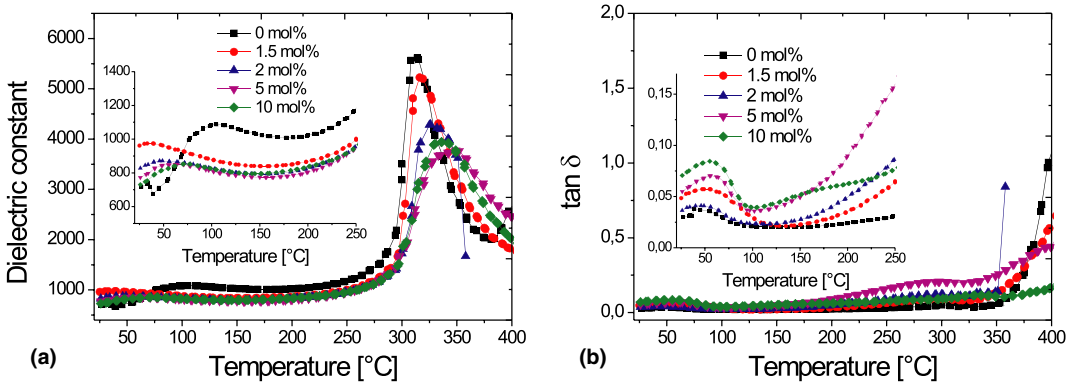

Fig. 3. Temperature-dependent plots of (a) dielectric constant and (b) dielectric loss (tan δ) measured at 100 kHz for KNNLST ceramics doped with different amounts of Mn.

Table VI. Density, Piezoelectric Coefficient (d^*_{33}), Remnant Strain (S_r) and Curie Temperature (T_c) for KNNLST Ceramics Modified with Different Amounts of Mn

Sample	Relative density (%)	d^*_{33} (pm/V)	P_r (μC/cm^2)	E_c (kV/cm)	S_r (%)	T_c (°C) X-ray	T_c (°C) Dielectric
0 mol%	93	338 ± 37	24	9.40	0.0824	340–360	310 ± 3
1.5 mol%	94	229 ± 18	20	~7.2	0.0358	300–320	316 ± 2
2 mol%	94	254 ± 13	18	~7.2	0.0461	–	326 ± 3
5 mol%	92	208 ± 27	13	~7.2	0.0143	340–360	335 ± 5
10 mol%	94	225 ± 20	14	~7.2	0.0334	320–340	336 ± 4

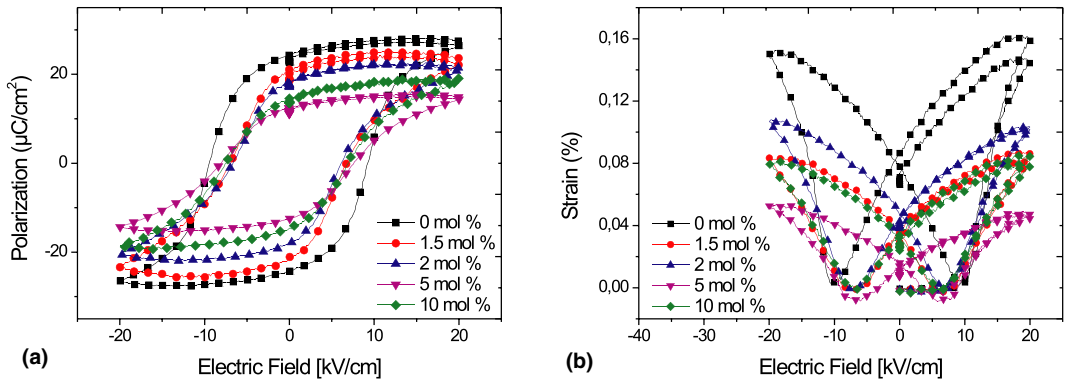

Fig. 4. (a) Polarization-electric field hysteresis curves and (b) strain – electric field hysteresis curves for KNNLST ceramics modified with different amounts of Mn.

This range of temperature corresponds to the two-phase coexistence region observed using X-ray diffraction. The dielectric constant values decrease with increasing Mn content whereas the dielectric loss increases with increasing Mn content. The high dielectric constant peak is observed with the undoped sample and this peak tends to broaden with increasing Mn content while the peak value decreases. For KNNLST-0 mol% Mn composition, the T_c is observed at ~310°C with a dielectric peak value of ~5636. For KNNLST-1.5 mol% Mn, the T_c is at 316°C with a dielectric peak value of 5225 while for KNNLST-2 mol% Mn, a T_c is at 326°C and a dielectric peak value of 4294 is obtained. The T_c value for KNNLST-5 mol% Mn is 335°C while the dielectric peak value is 3685. For KNNLST-10 mol% Mn, the T_c is 336°C and the dielectric peak value is 3940. A diffuse phase transition, which is characterized by extending the phase transition in a wide temperature interval around the T_c is observed for all the samples modified with Mn.

The polarization hysteresis curves for the samples modified with Mn are shown in Fig. 4(a). With an electric field of 20 kV/cm, saturation polarizations are attained for all the samples. The coercive field E_c and remnant polarization P_r values decrease with Mn addition. For KNNLST-0 mol% Mn sample, the P_r and E_c values are 24 μC/cm^2 and 9.4 kV/cm, respectively. E_c value of ~7.2 kV/cm are obtained for all the Mn-doped samples while the P_r values are 20, 18, 13, and 14 μC/cm^2 for 1.5, 2, 5, and 10 mol% of Mn, respectively. The bi-polar strain hysteresis curves for the samples are shown in Fig. 4(b). Good strain hysteresis curves are obtained for the samples and the addition of Mn resulted in a decrease in the obtained remnant strain S_r values. The S_r value for KNNLST-0 mol% Mn sample is 0.000824 and when Mn is added to the ceramic, the value decreases to ~0.0004. The details about the S_r values for the individual compositions is shown in Table VI.

The relative density, d^*_{33}, S_r, and T_c values for the samples are shown in Table IV. Addition of Mn did not lead to a significant difference in the relative density values of the samples as they are between 92% and 94% of their respective theoretical density.

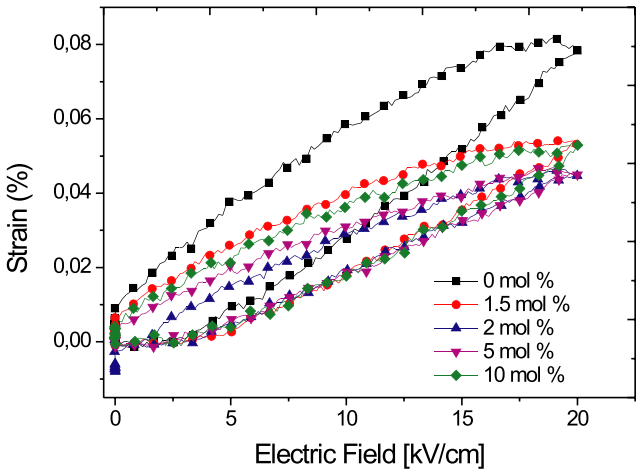

Fig. 5. Unipolar strain-electric field hysteresis curves for KNNLST ceramics modified with different amounts of Mn. The slopes of the plots were used to calculate the piezoelectric charge coefficient (d^*_{33}) values.

Figure 5 shows the unipolar strain hysteresis curves for the samples. The slope of the curves was used to calculate the d^*_{33} values. The highest value (338 ± 37 pm/V) is obtained with the KNNLST-0 mol% Mn sample and as Mn is added, the d^*_{33} values decrease to about 229 ± 18 pm/V for KNNLST-1.5 mol% Mn sample. The addition of more Mn to the sample did not lead to a significant change in the obtained d^*_{33} values.

IV. Discussion

The chemical analysis show that it is difficult to obtain exactly the same composition before and after sintering especially for elements like Li, K, and Sb, which are volatile. The addition of Mn stabilized the content of Sb, which implies that it reduces its volatilization rate during sintering.

The analysis of EPR results for KNN single crystals doped with Mn showed that it is incorporated to the B-site of the lattice.[24] It therefore acts as an acceptor dopant, which creates oxygen vacancies. When the Mn ions and O^{2-} ions combine, they form defect dipoles which cause pinning effects on domain switching and lead to hard ferroelectric effects in the samples. The results for KNNLST ceramics modified with Mn is more complex because the chemical analysis shows that in most cases, cation deficiency in both the A and B-sites of the lattice is observed. This implies that it is expected to have both hard and soft ferroelectric properties.

The X-ray diffraction patterns show that the sequence of phase transitions was not altered with Mn addition, but the temperature range of phase coexistence was lowered from 180°C to ~120°C. The possible reasons for phase coexistence in a material include the internal stress relaxation[35] and compositional fluctuations necessitated by inhomogeneity in the samples.[36] As the amount of Mn added to the KNNLST ceramic increased, the orthorhombic phase stabilizes and this implies that Mn in KNN ceramics is more stable with the orthorhombic lattice.

The dielectric properties of a ferroelectric material have contributions from both the intrinsic and extrinsic responses. The intrinsic contributions are mainly due to local atomic displacements within the unit cell that lead to the polarization of the material and depend on the domain orientation although the extrinsic contributions are mainly due to domain wall motions in the material due to an applied external electric field, which is higher than the E_c.[37] Only a small field was applied in this work and so only the intrinsic contribution is expected. The slightly higher dielectric constant and dielectric loss values for the Mn-doped samples at temperatures below 75°C are probably due to the coexistence of the orthorhombic and the tetragonal phase as shown in Fig. 1. For samples doped with Mn, broadening of the dielectric peaks is observed at the T_c possibly because of local compositional fluctuations, which create many competing dielectric maxima in the sample. The T_c values for the samples did not change with doping amounts probably due to the fact that the nature of the vacancies remains similar irrespective of the doping amount. This effect has been observed for Mn-doped $(Na_{0.5}K_{0.5})_{0.935}Li_{0.065}NbO_3$ ceramics by Zuo *et al.*[22] and in Mn-doped $0.98K_{0.5}Na_{0.5}NbO_3$–$0.02BiScO_3$ by Li *et al.*[38] The values of the T_c obtained using the dielectric constant and X-ray diffraction compares very well for the Mn-doped samples. For the undoped sample, however, the difference is big and this may be due to differences in preparation methods. The 20°C intervals used for the X-ray diffraction data acquisition could also contribute to the differences in T_c values since the onset of the cubic phase can begin at any temperature in the sample.

A combination of hard and soft ferroelectric effects is observed when Mn is used to dope the samples. The decreasing values of P_r indicate hard ferroelectric effects whereas the decreasing values of E_c indicate soft ferroelectric effects. This effect has also been reported for Mn-doped $0.98K_{0.5}Na_{0.5}NbO_3$–$0.02BiScO_3$ ceramics [38] and Mn-doped $(Bi_{1/2}Na_{1/2})TiO_3$–$BaTiO_3$ ceramics.[18] Increasing amount of Mn introduces more defects to the lattice, which hinders the switching of the domains leading to lower ferroelectric properties. The low values of d^*_{33}, S_r, and P_r obtained for KNNLST-5 mol% Mn ceramics may be related to the slightly lower density values.

V. Conclusion

The KNNLST ceramics modified with different amounts of Mn have been produced using the mixed-oxide synthesis method. Chemical analysis using OES-ICP spectroscopy shows that the intended and actual compositions vary slightly due to element volatility during sintering and impurity introduction during processing. The amount of Mn added to the sample did not affect the sequence of phase transition, but decreases the temperature range of phase coexistence from 180°C to 120°C. The orthorhombic phase is stabilized between 27°C and 80°C with increasing amount of Mn added to the sample. Both the dielectric constant and dielectric loss values increase with small amounts of Mn and decrease with increasing Mn amount. The T_c did not decrease with the amount of Mn present probably because the nature of the defects is similar irrespective of the amount of dopant. Good polarization and strain hysteresis curves and high piezoelectric coefficients were obtained for all the samples. The highest d^*_{33} value was for the sample without Mn, which indicates that Mn introduces vacancies, which inhibit the domains to switch easily when an electric field is applied.

Acknowledgments

Supported by the Deutsche Forschungsgemeinschaft (DFG), under grant no. SCHN 372/16-2 and Bundesministerium für Bildung und Forschung (BMBF), under grant no. 05K10ODA.

References

[1]Y. Guo, K.-I. Kakimoto, and H. Ohsato, "Dielectric and Piezoelectric Properties of Lead-Free $(Na_{0.5}k_{0.5})Nbo_3$–$Srtio_3$ Ceramics," *Sol. State Commun.*, **129** [5] 279–84 (2004).

[2]Y. Guo, K.-I. Kakimoto, and H. Ohsato, "Phase Transitional Behavior and Piezoelectric Properties of $(Na_{0.5}k_{0.5})Nbo_3$–$Linbo_3$ Ceramics," *Appl. Phys. Lett.*, **85** [18] 4121–3 (2004).

[3]H. E. Mgbemere, R.-P. Herber, and G. A. Schneider, "Investigation of the Dielectric and Piezoelectric Properties of Potassium Sodium Niobate Ceramics Close to the Phase Boundary at $(K_{0.35}na_{0.65})Nbo_3$ and Partial Substitutions with Lithium and Antimony," *J. Eur. Ceram. Soc.*, **29**, 3273–8 (2009).

[4]H. E. Mgbemere, G. A. Schneider, and T. A. Stegk, "Effect of Antimony Substitution for Niobium on the Crystal Structure, Piezoelectric and Dielectric Properties of $(K_{0.5}Na_{0.5})NbO_3$ Ceramics," *Funct. Mat. Lett.*, **3** [1] 25–30 (2010).

[5]N. Klein, E. Hollenstein, D. Damjanovic, H. J. Trodahl, and N. Setter, "A study of the Phase Diagram of (K,Na,Li)NbO_3 Determined by Dielectric and Piezoelectric Measurements, and Raman Spectroscopy," *J. Appl. Phys.*, **102** [1] 014112, 8pp (2007).

[6]K. Chen, G. Xu, D. Yang, X. Wang, and J. Li, "Dielectric and Piezoelectric Properties of Lead-Free 0.95($K_{0.5}Na_{0.5}$)NbO_3–0.05$LiNbO_3$ Crystals Grown by the Bridgman Method," *J. Appl. Phys.*, **101** [4] 044103, 4pp (2007).

[7]D. Lin, K. W. Kwok, and H. L. W. Chan, "Phase Transition and Electrical Properties of ($K_{0.5}Na_{0.5}$)($Nb_{1-x}Ta_x$)O_3 Lead-Free Piezoelectric Ceramics," *Appl. Phys. A*, **91** [1] 167–71 (2008).

[8]H. Tian, Z. Zhou, D. Gong, H. Wang, D. Liu, and Y. Jiang, "Growth and Optical Properties of Paraelectric $K_{1-y}Na_yTa_{1-x}Nb_xO_3$ Single Crystals," *Appl. Phys. B*, **91** [1] 75–8 (2008).

[9]Y. Saito and H. Takao, "High Performance Lead-Free Piezoelectric Ceramics in the (K,Na)NbO_3-$LiTaO_3$ Solid Solution System," *Ferroelectrics*, **338**, 17–32 (2006).

[10]Y. Zhen and J.-F. Li, "Abnormal Grain Growth and New Core–Shell Structure in (K,Na)NbO_3-Based Lead-Free Piezoelectric Ceramics," *J. Am. Ceram. Soc.*, **90** [11] 3496–502 (2007).

[11]F. Zhu, T. A. Skidmore, A. J. Bell, T. P. Comyn, C. W. James, M. Ward, and S. J. Milne, "Diffuse Dielectric Behaviour in $Na_{0.5}K_{0.5}NbO_3$–$LiTaO_3$–$BiScO_3$ Lead-Free Ceramics," *Mater. Chem. Phys.*, **129**, 411–7 (2011).

[12]J. Wu, D. Xiao, Y. Wang, J. Zhu, P. Yu, and Y. Jiang, "Compositional Dependence of Phase Structure and Electrical Properties in ($K_{0.42}Na_{0.58}$)NbO_3-$LiSbO_3$ Lead-Free Ceramics," *J. Appl. Phys.*, **102** [11] 114113, 5pp (2007).

[13]Y. Saito, H. Takao, T. Tani, T. Nonoyama, K. Takatori, T. Homma, T. Nagaya, and M. Nakamura, "Lead-Free Piezoceramics," *Nature*, **432**, 84–7 (2004).

[14]H. T. Langhammer, T. Mueller, K.-H. Felgner, and H.-P. Abicht, "Crystal Structure and Related Properties of Manganese-Doped Barium Titanate Ceramics," *J. Am. Ceram. Soc.*, **83** [3] 605–11 (2000).

[15]J.-Y. Kim, C.-R. Song, and H.-I. Yoo, "Mn-Doped $BaTiO_3$: Electrical Transport Properties in Equilibrium State," *J. Electroceram.*, **1** [1] 27–39 (1997).

[16]J.-H. Park, J.-G. Park, B.-K. Kim, H.-J. Je, and Y. Kim, "Effect of MnO_2 Addition on the Piezoelectric Properties in $Pb(Mg_{1/3}Nb_{2/3})O_3$ Relaxor Ferroelectrics," *Mater. Res. Bull.*, **37** [2] 305–11 (2002).

[17]X.-J. Li, Q. Wang, and Q.-L. Li, "Effects of MnO_2 Addition on Microstructure and Electrical Properties of $(Bi_{0.5}Na_{0.5})_{0.94}Ba_{0.06}TiO_3$ Ceramics," *J. Electroceram.*, **20** [2] 89–94 (2008).

[18]G. Fan, W. Lu, X. Wang, and F. Liang, "Effects of Manganese Additive on Piezoelectric Properties of $(Bi_{1/2}Na_{1/2})TiO_3$–$BaTiO_3$ Ferroelectric Ceramics," *J. Mater. Sci.*, **42** [2] 472–6 (2007).

[19]E. Aksel, P. Jakes, E. Erdem, D. M. Smyth, A. Ozarowski, J. V. Tol, J. L. Jones, and R.-A. Eichel, "Processing of Manganese-Doped $[Bi_{0.5}Na_{0.5}]TiO_3$ Ferroelectrics: Reduction and Oxidation Reactions During Calcination and Sintering," *J. Am. Ceram. Soc.*, **94** [5] 1363–7 (2011).

[20]D. Lin, K. W. Kwok, and H. L. W. Chan, "Effects of MnO_2 on the Microstructure and Electrical Properties of 0.94($K_{0.5}Na_{0.5}$)NbO_3–0.06$Ba(Zr_{0.05}Ti_{0.95})O_3$ Lead-Free Ceramics," *Mater. Chem. Phys.*, **109** [2–3] 455–8 (2008).

[21]D. Lin, K. W. Kwok, and H. L. W. Chan, "Piezoelectric and Ferroelectric Properties of $K_xNa_{1-x}NbO_3$ Lead-Free Ceramics with MnO_2 and CuO Doping," *J. Alloys Comp.*, **461** [1–2] 273–8 (2008).

[22]R. Zuo, J. Fu, S. Su, X. Fang, and J.-L. Cao, "Electrical Properties of Manganese Modified Sodium Potassium Lithium Niobate Lead-Free Piezoelectric Ceramics," *J. Mater. Sci.: Mater. Electron.*, **20** [3] 212–6 (2009).

[23]P. Bomlai, P. Sinsap, S. Muensit, and S. J. Milne, "Effect of MnO on the Phase Development, Microstructures, and Dielectric Properties of 0.95$Na_{0.5}K_{0.5}NbO_3$–0.05$LiTaO_3$ Ceramic," *J. Am. Ceram. Soc.*, **91** [2] 624–7 (2008).

[24]Y. Kizaki, Y. Noguchi, and M. Miyayama, "Defect Control for Low Leakage Current in $K_{0.5}Na_{0.5}NbO_3$ Single Crystals," *Appl. Phys. Lett.*, **89** [14] 142910, 3pp (2006).

[25]Y. Noguchi and M. Miyayama, "Effect of Mn Doping on the Leakage Current and Polarization Properties in $K_{0.14}Na_{0.86}NbO_3$ Ferroelectric Single Crystals," *J. Ceram. Soc. Jpn.*, **118**, 711–6 (2010).

[26]D. Lin, Z. Li, S. Zhang, Z. Xu, and X. Yao, "Influence of MnO_2 Doping on the Dielectric and Piezoelectric Properties and the Domain Structure in ($K_{0.5}Na_{0.5}$)NbO_3 Single Crystals," *J. Am. Ceram. Soc.*, **93** [4] 941–4 (2010).

[27]M. Knapp, V. Joco, C. Baehtz, H. H. Brecht, A. Berghaeuser, H. Ehrenberg, H. v. Seggern, and H. Fuess, "Position-Sensitive Detector System OBI for High Resolution X-ray Powder Diffraction Using On-Site Readable Image Plates," *Nucl. Instrum. Methods Phys. Res. A*, **521** [2–3] 565–70 (2004).

[28]M. Knapp, C. Baehtz, H. Ehrenberg, and H. Fuess, "The Synchrotron Powder Diffractometer at Beamline B2 at HASYLAB/DESY: Status and Capabilities," *J. Synchrotron Rad.*, **11** [4] 328–34 (2004).

[29]J. Rodríguez-Carvajal, "Recent Advances in Magnetic Structure Determination by Neutron Powder Diffraction," *Physica B*, **192** [1–2] 55–69 (1993).

[30]B. V. Laar and W. B. Yelon, "The Peak in Neutron Powder Diffraction," *J. Appl. Cryst.*, **17**, 47–54 (1984).

[31]L. W. Finger, D. E. Cox, and A. P. Jephcoat, "A Correction for Powder Diffraction Peak Asymmetry Due to Axial Divergence," *J. Appl. Cryst.*, **27**, 892–900 (1994).

[32]L. W. Finger, "PROFVAL: Functions to Calculate Powder-Pattern Peak Profiles with Axial Divergence Asymmetry," *J. Appl. Cryst.*, **31**, 111 (1998).

[33]P. W. Stephens, "Phenomenological Model of Anisotropic Peak Broadening in Powder Diffraction," *J Appl. Cryst.*, **32**, 281–9 (1999).

[34]H. E. Mgbemere, M. Hinterstein, R. P Fernandes, and G. A. Schneider, "Temperature-Dependent Synchrotron Powder Diffraction Phase Studies of ($K_{0.37}Na_{0.52}Li_{0.03}$)($Nb_{0.87}Ta_{0.1}Sb_{0.03}$)$O_3$ Ferroelectric Ceramics," *Z. Kristallogr.*, **226** [2] 138–44 (2011).

[35]T. Kala, "Contribution to the Study of Tetragonal and Rhombohedral Phase Coexistence in the $PbZrO_3$-$PbTiO_3$ System," *Phys. stat. sol. (a)*, **78** [1] 277–82 (1983).

[36]J. Frantti, S. Ivanov, S. Eriksson, H. Rundlöf, V. Lantto, J. Lappalainen, and M. Kakihana, "Phase Transitions of $Pb(Zr_xTi_{1-x})O_3$ Ceramics," *Phys. Rev. B*, **66** [6] 064108, 15pp (2002).

[37]Q. M. Zhang, H. Wang, N. Kim, and L. E. Cross, "Direct Evaluation of Domain-Wall and Intrinsic Contributions to the Dielectric and Piezoelectric Response and their Temperature Dependence on Lead Zirconate-Titanate Ceramics," *J. Appl. Phys.*, **75** [1] 454–9 (1994).

[38]X. Li, M. Jiang, J. Liu, J. Zhu, X. Zhu, J. Zhu, and D. Xiao, "Enhanced Piezoelectric Properties in Mn-Doped 0.98$K_{0.5}Na_{0.5}NbO_3$–0.02$BiScO_3$ Lead-Free Ceramics," *J. Am. Ceram. Soc.*, **92** [7] 1625–8 (2009). □